

Singular basins in multiscale systems

S. Yanchuk^{1,2}, S. Wieczorek¹, H. Jardón-Kojakhmetov³, and H. Alkhayouon¹

¹*School of Mathematical Sciences, University College Cork, Western Road, Cork T12 XF62, Ireland*

²*Potsdam Institute for Climate Impact Research,*

P.O Box 6012 03, 14412 Potsdam, Germany and

³*Johann Bernoulli Institute for Mathematics and Computer Science,*

University of Groningen, P.O. Box 407, 9700 AK, Groningen, The Netherlands

(Dated: January 6, 2026)

Real-world complex systems often evolve on different timescales and possess multiple coexisting stable states. Whether or not a system returns to a given stable state after being perturbed away from it depends on the shape and extent of its basin of attraction. In this Letter, we show that basins of attraction in multiscale systems can exhibit special geometric properties in the form of universal *singular funnels*. We use the term *singular basins* to refer to basins of attraction with singular funnels. We show that singular basins occur robustly in a range of dynamical systems: the normal form of a pitchfork bifurcation with a slowly changing parameter, an adaptive active rotator, and an adaptive network of phase rotators. Although singular funnels are narrow, they can extend to different parts of the phase space and, unexpectedly, impact the resilience of the system to disturbances. Crucially, the presence of a singular funnel may prevent the usual dimensionality reductions in the limit of large timescale separation, such as quasi-static approximation, adiabatic elimination or time-averaging of the fast variables

Complex real-world systems are characterized by *multistability*, i.e. when given different initial conditions, the same system can end up with notably different asymptotic behavior. Examples of multistability can be found in epileptic and neuronal models [1–4], reservoir computers [5], lasers [6–8], and climate [9–11], to name a few. The analysis and control of multistability-related phenomena has therefore been the subject of many studies [12–15]. An important question in multistable systems concerns the interplay between different stable states and possible transitions between them. In the context of cell differentiation, for instance, transitions between attractors by a perturbation correspond to the reprogramming of cells [16]. One notable approach addressing the above challenges is the concept of basin stability [17, 18], which represents the likelihood of reaching a particular stable state starting from random initial conditions. This likelihood can be estimated by the volume of the basin of attraction of a stable state, in other words, the proportion of initial conditions in the phase space that evolve into that state over time. More importantly, the geometry of the basins of attraction determines the resilience of a system to perturbations [19, 20]. Therefore, studying basins of attraction of different stable states, whether their relative volumes or, more broadly, their geometries, is crucial for understanding and controlling multistable systems.

In addition to having multiple stable states, it is also common for real-world systems to evolve on *multiple timescales*, which give rise to a variety of nonlinear phenomena [21–25]. An important example of a multi-scale system is an adaptive dynamical network, where the adaptation is much slower than the node dynamics [26–31]. Such systems are challenging because they are high-dimensional, and can exhibit high multistability with a large number of coexisting stable states [32]. The study

of the basins of attraction for multiscale systems is a largely unexplored area of research, and revealing the properties of the basins arising from the interplay of multiple timescales is an intriguing and important task.

A number of useful techniques have been developed for analysing mathematical models of multiscale systems with two distinct timescales, also known as slow-fast systems [33–36]. These include adiabatic elimination, quasistatic approximation, and averaging, which allow the elimination of the fast variables by taking into account their effective averaged contribution to the slow dynamics [37–39].

This Letter reports specific properties of basins in slow-fast systems that arise from their multiscale separation. We show that these basins can contain *singular funnels* (SFs) in the form of tunnels that become increasingly narrow as the timescale separation grows. Due to this vanishing property, we refer to basins containing SFs as *singular basins*. In systems with SFs, adiabatic elimination or the quasistatic approximation causes the SFs to disappear and, consequently, eliminates the possibility of reaching a given steady state from certain regions of phase space. Therefore, one must be cautious when extrapolating the resilience properties of the full system from those of a reduced one, whether obtained via quasistatic approximation, adiabatic elimination, or averaging.

For example, if an averaged system has a bistable potential with two stable states, the basins of attraction of these states are clearly separated. In other words, there exists a threshold value of the slow variable such that, on each side of it, the system evolves toward a different steady state. However, when the fast subsystem is taken into account, SFs enable convergence to the same steady state from both sides of the threshold value of the slow variable, even when the separation of timescales is

arbitrarily large. From the perspective of the reduced system, this appears as a “tunnelling” from one state to another, Fig. 1(b).

We show the singular basin in different classes of systems: a pitchfork bifurcation normal form with a slowly changing parameter, an active rotator with an adaptive frequency, and an adaptive dynamical network of active rotators. We further show that the phenomenon is robust to parameter changes and exhibits universal scaling with increasing timescale separation in small dimensions. We conclude that singular basins are common in multiscale systems, and specify the main conditions under which this phenomenon occurs.

We first present the singular basin in a normal form for the pitchfork bifurcation, where the bifurcation parameter is slowly changing. The pitchfork bifurcation is one of the few generic mechanisms for stability exchange in dynamical systems, and its normal form equation is $\dot{x}(t) = x(\mu - x^2)$ in the supercritical case [40]. Here x is a dynamical variable and μ a parameter. We restrict the normal form system to non-negative x values, which is appropriate for many applications, for example, when the variable x denotes a population size or laser intensity. Then, the system has a single stable steady state for all parameters μ , $x^* = 0$ for $\mu \leq 0$, and $x^* = \sqrt{\mu}$ for $\mu \geq 0$. In a more compact form, one can write the stable equilibrium as $x^* = \sqrt{H(\mu)\mu}$, where $H(\mu)$ is the Heaviside step function $H(\mu) = 0$ for $\mu < 0$ and $H(\mu) = 1$ for $\mu \geq 0$. The slow dynamics is given by a linear adaptation of the bifurcation parameter μ , resulting in the following system

$$\dot{x}(t) = x(\mu - x^2), \quad (1)$$

$$\dot{\mu}(t) = \varepsilon(-\mu + ax - b), \quad (2)$$

where ε is a small positive parameter, and $a, b > 0$ are parameters determining the adaptation rule. Under the condition $a > 2\sqrt{b}$, system (1-2) possesses three equilibria: two stable equilibria e_0 and e_2 , and one saddle point e_1 as shown in Fig. 1(a), see calculations in Supplemental Material [41].

Since the fast subsystem (1) possesses a unique stable equilibrium $x^*(\mu) = \sqrt{H(\mu)\mu}$ for all values of the slow variable μ , we apply the adiabatic elimination procedure, i.e., substitute $x^*(\mu)$ into (2) and obtain the reduced slow system

$$\dot{\mu} = \varepsilon f(\mu), \quad (3)$$

with $f(\mu) = -\mu + a\sqrt{H(\mu)\mu} - b$ and the corresponding potential $U(\mu) = -\int f(\mu)d\mu = \mu^2/2 + b\mu - 2a\mu\sqrt{H(\mu)\mu}/3$ as shown in Fig. 1(b). Hence, the adiabatic elimination reduces system (1-2) to a simple bistable potential system for the slow variable μ .

In the reduced system (3), the fast dynamics is eliminated and the attraction basins of the stable equilibria μ_0 and μ_1 are separated by μ_2 . Therefore, all states of (3) initially started with $\mu < \mu_2$ tend to μ_0 over time, while all $\mu > \mu_2$ tend to μ_1 . This clear division of basins by

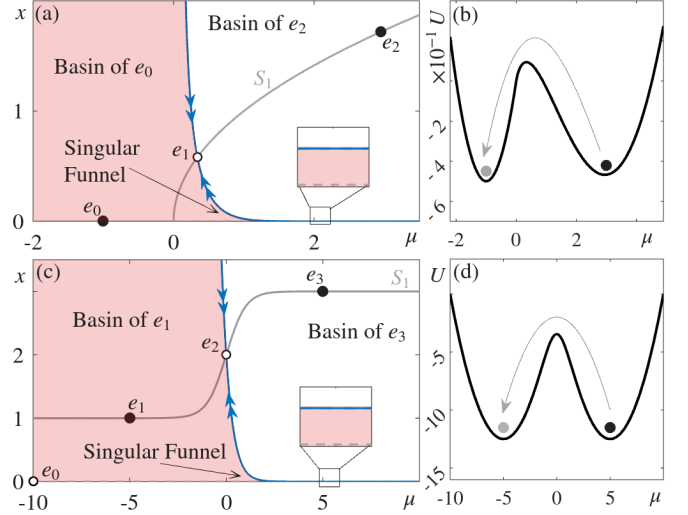


FIG. 1. (a-b): Singular basin and singular funnel (SF) in a pitchfork normal form (1-2) with slowly adapting parameter μ . (a) Phase space of the system with two coexisting stable equilibria e_0 and e_2 and the corresponding basins of attraction. The red (white) region is the basin of attraction of e_0 (e_2). SF is observed near the $x = 0$ axis, it extends to arbitrarily large μ values and decreases exponentially in width. Parameters: $a = 3$, $b = 2$, and $\varepsilon = 0.1$. (b) The bistable potential of the corresponding slow system after adiabatic elimination of the fast variable (equivalently, reduction to the stable critical manifold). (c-d): Same for system (26). Parameters: $a = 5$, $b = 10$, and $\varepsilon = 0.1$.

$\mu = \mu_2$ is not present in the original slow-fast system (1-2) even for an arbitrary large time-scale separation $1/\varepsilon$. Figure 1(a) shows the basins of attraction of the stable states e_0 and e_2 . It can be seen that states with arbitrarily large μ can converge to the left equilibrium e_0 over time when the initial conditions are chosen in the SF, which is a small stripe close to $x = 0$. This funnel-like part of the attraction basin has an exponentially small width as ε decreases, leaving the possibility of “tunnelling” towards the e_0 state. The SF clearly restricts the applicability of the adiabatic elimination.

One might suspect that the failure of a global adiabatic elimination is caused by the degenerate point at $(\mu, x) = (0, 0)$ in the pitchfork normal form (1-2). However, to demonstrate that this is not the case, we present the singular basin for a modified model:

$$\begin{aligned} \dot{x}(t) &= x(\tanh \mu + 2 - x), \\ \dot{\mu}(t) &= \varepsilon(-\mu + ax - b) \end{aligned} \quad (4)$$

in Fig. 1(c-d). The singular basin appears there without any degenerate point.

An exponentially narrow SF observed in the paradigmatic models (1-2) and (26) appears to be characteristic for more complex classes of slow-fast systems. We will demonstrate this for an adaptive phase rotator model and an adaptive network of coupled phase rotators.

The fast-slow adaptive phase rotator has the form [42]

$$\dot{\varphi}(t) = \omega + \mu - \sin \varphi, \quad (5)$$

$$\dot{\mu}(t) = \epsilon(-\mu + \eta(1 - \sin(\varphi + \alpha))), \quad (6)$$

where φ is a phase variable and μ accounts for a slow self-adjustment of the oscillator frequency. Although system (5–6) has the same dimension as the normal form (1–2), the fast variable φ can describe periodic rotations. In particular, the fast subsystem (5) has a pair of stable and unstable equilibria for $|\omega + \mu| < 1$ and a rotating solution for $|\omega + \mu| > 1$ [43]. At the point $|\omega + \mu| = 1$, the fast subsystem undergoes a "saddle-node on an invariant curve" bifurcation [42, 44]. Hence the fast subsystem (5) has a single stable attractor for all fixed values of μ , which is an equilibrium for $|\omega + \mu| \leq 1$ and a rotation for $|\omega + \mu| > 1$.

The adaptive phase oscillator (5–6) can also be reduced to the form (3) after an elimination of the fast timescale. This is achieved by averaging over the fast rotations for $|\omega + \mu| > 1$ and by adiabatic elimination for the remaining values of μ on the single stable equilibrium. The corresponding function $f(\mu)$ of the reduced system (3) can be calculated explicitly:

$$f(\mu) = -\mu + \eta(1 - (\mu + \omega) \cos \alpha - \Omega(\mu)), \quad (7)$$

where

$$\Omega(\mu) = \begin{cases} \sqrt{1 - (\mu + \omega)^2} \cdot \sin \alpha, & |\mu + \omega| \leq 1 \\ \sqrt{(\omega + \mu)^2 - 1} \cdot \cos \alpha, & |\mu + \omega| > 1. \end{cases}$$

The details of the derivation can be found in the Supplemental Material [41].

We consider the case when system (5–6) possesses two coexisting attractors: a stable equilibrium e_1 and a stable rotation γ_c , see Fig. 2(a,b). This bistability occurs for a large set of parameters $(\varepsilon, \alpha, \eta)$, which is described in detail in Supplemental Material [41]. The reduced system (3), with the right-hand side given by equation (7), is also bistable in this case, and its potential is shown in Fig 2(d). Here μ_1, μ_c , and μ_2 are the μ -coordinates of the equilibrium e_1 , the rotation γ_c in the limit $\varepsilon \rightarrow 0$, and the saddle point e_2 , respectively.

The singular basin of the adaptive phase oscillator (5–6) is shown in Figures 2(a) and (b). The SF has an exponentially decreasing width for small ε and extends into the region of negative μ . This creates a channel that allows for initial conditions with arbitrary μ and selected φ to be attracted to the rotating attractor γ_c , which is impossible in the framework of the averaged system (3).

Next, we provide details of how the boundaries of the SF are formed in Fig. 2(a,b). As in the pitchfork normal form case (1–2), these boundaries consist of orbits attracted to the saddle equilibrium e_2 (the stable manifolds). Tracking these orbits backwards in time reveals that they pass close to the unstable equilibria of the fast system (the dashed part of S in Fig. 2(a,b)), which is

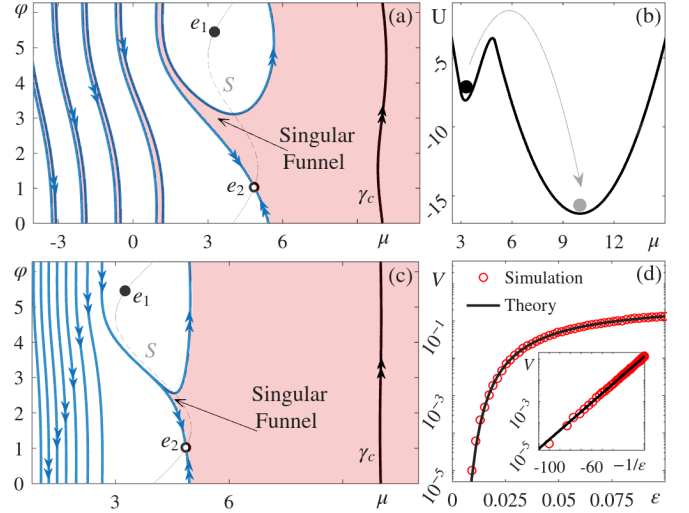


FIG. 2. Singular basin and singular funnels in an adaptive phase-oscillator (5–6). (a) and (c): The red shaded area is the basin of attraction of the limit cycle γ_c , the white area is the basin of attraction of the equilibrium e_1 . The boundary of the two basins is given by the stable manifold of the saddle equilibrium e_2 (blue lines). (b): The bistable potential of the reduced system (3,7) after averaging and adiabatic elimination of the fast variable. (d) The volume of the singular funnel of γ_c for $-10 \leq \mu \leq 0$ as a function of ε . Red circles: the volume computed using Monte Carlo simulation [41]. Black line: the volume as given by equation (8). Other parameters: $\eta = 10$, $\omega = -4$. (a): $\alpha = \pi/2$, $\varepsilon = 0.1$, (c): $\alpha = \pi/2$, $\varepsilon = 0.01$.

also known as the critical manifold [21]. Since this part of the critical manifold is stable in backward time, the two SF boundaries are exponentially attracted, causing the SF to become exponentially narrow. After the SF has passed S , it undergoes further rotations and extends to arbitrarily negative μ , maintaining the same exponentially narrow width.

For the considered systems with singular basins, we can obtain the scaling of the SF phase volume as a function of ε and estimate how quickly it vanishes as ε approaches 0. In all cases, the motion along the trajectories, which correspond to the SF boundaries, is slow and its speed is proportional to ε along the critical manifold S , so the time they spend close to a finite piece of length L of S scales as L/ε . The width δ of the SF is determined by two trajectories that pass close to S (blue trajectories in Fig. 2) and, hence, δ decreases exponentially as time goes backwards. Therefore, this width can be estimated as $\delta \sim \exp(-L\lambda/\varepsilon)$ at the moment when the boundaries leave the critical manifold S (or a section of it of length L). Here λ is an effective repulsion rate at S , which corresponds to the attraction in the reverse time. These arguments lead to the following expected scaling for the volume of a SF:

$$V(\varepsilon) \sim \exp(-C\varepsilon^{-1}), \quad C > 0. \quad (8)$$

The scaling (8) clearly holds for the normal form sys-

tem (1–2) and system (26). Furthermore, the rotator system (5–6) exhibits this scaling too, as shown in Fig. 2(c). The basin scaling (8) is expected to hold for large classes of slow-fast systems, at least in low dimensions, as the arguments leading to (8) are based on the rather general geometric structure of the basin boundaries. However, as we will see below, this scaling may sometimes fail to accurately describe singular basins in high-dimensional systems.

Singular basin is a robust phenomenon. This is due to the fact that its ingredients persist under small parameter changes. This applies to the stable manifolds of the saddle equilibria and the coexisting attractors. We illustrate the parameter region of the singular basin and the possible mechanisms of its destruction for system (5–6) in the Supplemental Material [41].

A higher-dimensional class of systems, in which singular basins can be observed, is the mean-field coupled active rotators

$$\dot{\varphi}_i = \omega_i + \mu - \sin \varphi_i + \frac{\kappa}{N} \sum_{j=1}^N \sin(\varphi_j - \varphi_i), \quad (9)$$

$$\dot{\mu} = \epsilon(-\mu + \eta(1 - X)), \quad (10)$$

where $i = 1, \dots, N$ and $X = \frac{1}{N} \sum_{j=1}^N \sin(\varphi_j + \alpha)$. In this system, the frequencies of the individual rotators are adapted globally by the slow variable μ , and μ is driven by the mean-field X . This could be viewed as an interaction with the environment. In contrast to the extensively studied system of coupled rotators without adaptation [15, 45–51], the adaptive system (9–10) contains multiple timescales. Adaptive systems of a similar nature have been shown to exhibit distinct dynamical properties such as canard cascading [23, 52], emergent excitability [53], and others [54–56].

Figures 3 and 4 show singular basins and their scaling in systems of $N = 2$ and $N = 10$ rotators, respectively. Both systems feature the coexistence of two attractors: one stable equilibrium and another rotating periodic or quasi-periodic attractor. Consequently, the corresponding averaged system exhibits a bistable potential, as shown in Fig. 3(a). This bistability is caused by the phase-space structures similar to those in the single adaptive rotator. However, a detailed description of these structures is beyond the scope of this letter.

Figure 3(a) shows a bistable potential calculated by averaging system (9) with $N = 2$ oscillators. Two-dimensional cross-sections of the corresponding singular basin for fixed values of φ_1 and μ values are illustrated in Figs. 3(b) and (d), respectively. The SF volume vanishes as ϵ decreases; figure 3(c) demonstrates this for different values of the detuning parameter $\Delta_\omega = \omega_1 - \omega_2$. We observe that the scaling of the dependence $V(\epsilon)$ agrees with the rule (8) for some values of Δ_ω ($\Delta_\omega = 0.6$), while for other values, it exhibits a non-monotonic resonant-like behavior ($\Delta_\omega = 1$ or $\Delta_\omega = 2.2$). Hence, we conclude that the scaling (8) can fail for the SF in higher-dimensional

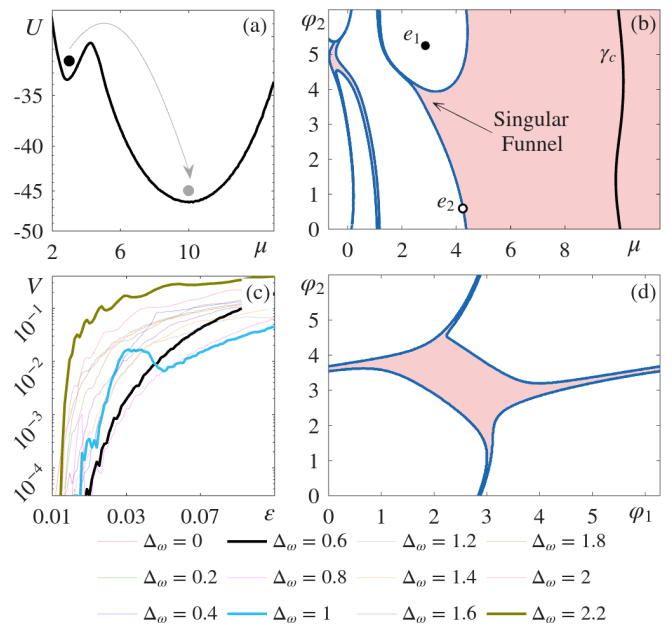


FIG. 3. Illustration of the singular basin in system (9) of $N = 2$ coupled phase rotators. (a) The bistable potential of the averaged system. (b) A two-dimensional cross-section of the basin of the full slow-fast system. The notations are the same as in Fig. 2. The cross-section for fixed $\varphi_1 = 1.2461$. (c) The volume of the singular funnel for γ_c , limited to $\mu \in [-10, 0]$, as a function of ϵ for different values of the parameter $\Delta_\omega = \omega_1 - \omega_2$. (d) The cross-section of the basin for fixed $\mu = 2.86$.

systems due to the more complex structure of the basin boundaries.

Finally, the singular basin for the system of $N = 10$ adaptively coupled rotators (9) is demonstrated in Fig. 4. The figure shows how the SF volume vanishes as a function of ϵ . Additionally, two trajectories are shown in Fig. 4(b): one starts from the SF and enters rotating motion (red), and one starts very close by that converges to a stable equilibrium.

In summary, we described the phenomenon of a singular basin and a singular funnel, which is characteristic of a wide range of slow-fast systems. The presence of a singular basin hinders a reliable timescale reduction of multiscale systems, even when the timescales are significantly different. More specifically, while systems reduced by adiabatic elimination or averaging can exhibit a coexistence of different states with clearly separated basins of attraction, the fast timescale of the original system can lead to the dynamics that is not predicted by the reduced system. This unexpected dynamics looks like a tunnelling transition from one attractor to another when only the reduced system is considered. To understand this phenomenon in greater detail, we developed minimal normal form systems. Additionally, we have demonstrated that singular basins can be observed in higher-dimensional mean-field coupled rotators. While our study focused on bistability,

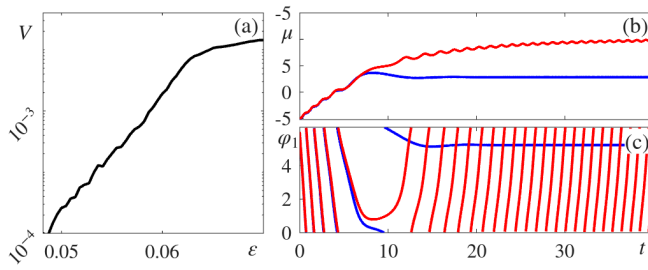


FIG. 4. Evidence of the singular basin in the system (9) of ten coupled oscillators. (a) Scaling of the singular basin volume $\omega_i = -4 + (i-1)/9$, $i = 1, \dots, 10$. Parameters: $\eta = 10$, $\alpha = \pi/2$, $\kappa = 1$. (b) Examples of the trajectories: The red trajectory starts from the SF and approaches a rotating attractor asymptotically. The blue trajectory converges to an equilibrium. Initial conditions are $\varphi_i(0) = 6$, $i = 1, \dots, 10$, $\mu(0) = -5$ for the red trajectory, and $\mu(0) = -5.1$ for the blue trajectory.

future research involving more than two coexisting attractors and possible tunneling between them would be of interest.

Intriguingly, while any model of a real-world system is necessarily an approximation involving the omission or reduction of faster timescales, our results offer a new perspective on the unexpected transitions of these systems, such as tunnelling between two stable states, which could be triggered by the omitted timescales.

ACKNOWLEDGMENTS

This work emanated from the research funded by Taighde Éireann—Research Ireland (Grant No. FFP-A/12066).

[1] V. Jirsa, H. Wang, P. Triebkorn, M. Hashemi, J. Jha, J. Gonzalez-Martinez, M. Guye, J. Makhlova, and F. Bartolomei, Personalised virtual brain models in epilepsy, *The Lancet Neurology* **22**, 443 (2023).

[2] W. Gerstner, W. M. Kistler, R. Naud, and L. Paninski, *Neuronal Dynamics* (Cambridge, 2014).

[3] K. J. Pfeifer, J. A. Kromer, A. J. Cook, T. Hornbeck, E. A. Lim, B. J. P. Mortimer, A. S. Fogarty, S. S. Han, R. Dhall, C. H. Halpern, and P. A. Tass, Coordinated Reset Vibrotactile Stimulation Induces Sustained Cumulative Benefits in Parkinson’s Disease, *Frontiers in Physiology* **12**, 624317 (2021).

[4] T. Manos, S. Diaz-Pier, and P. A. Tass, Long-Term Desynchronization by Coordinated Reset Stimulation in a Neural Network Model With Synaptic and Structural Plasticity, *Frontiers in Physiology* **12**, 716556 (2021).

[5] A. Flynn, V. A. Tsachouridis, and A. Amann, Multifunctionality in a reservoir computer, *Chaos: An Interdisciplinary Journal of Nonlinear Science* **31**, 013125 (2021).

[6] L. Jaurigue, B. Krauskopf, and K. Lüdge, Multipulse dynamics of a passively mode-locked semiconductor laser with delayed optical feedback, *Chaos* **27**, 114301 (2017).

[7] S. Wieczorek, B. Krauskopf, T. B. Simpson, and D. Lenstra, The dynamical complexity of optically injected semiconductor lasers, *Phys. Rep.* **416**, 1 (2005).

[8] S. Yanchuk, S. Ruschel, J. Sieber, and M. Wolfrum, Temporal dissipative solitons in time-delay feedback systems, *Physical Review Letters* **123**, 053901 (2019).

[9] H. Alkhayouon, P. Ashwin, L. C. Jackson, C. Quinn, and R. A. Wood, Basin bifurcations, oscillatory instability and rate-induced thresholds for atlantic meridional overturning circulation in a global oceanic box model, *Proceedings of the Royal Society A* **475**, 20190051 (2019).

[10] C. Quinn, J. Sieber, A. S. von der Heydt, and T. M. Lenton, The mid-pleistocene transition induced by delayed feedback and bistability, *Dynamics and Statistics of the Climate System* **3**, dzy005 (2018).

[11] K. Slyman, E. Fleurantin, and C. K. Jones, Tipping mechanisms in a carbon cycle model, *Chaos: An Interdisciplinary Journal of Nonlinear Science* **35** (2025).

[12] A. N. Pisarchik and U. Feudel, Control of multistability, *Physics Reports* **540**, 167 (2014).

[13] P. Ebrahizadeh, M. Schiek, and Y. Maistrenko, Mixed-mode chimera states in pendula networks, *Chaos: An Interdisciplinary Journal of Nonlinear Science* **32**, 103118 (2022).

[14] T. Malashchenko, A. Shilnikov, and G. Cymbalyuk, Six types of multistability in a Neuronal model based on slow calcium current, *PLoS ONE* **6**, 10.1371/journal.pone.0021782 (2011).

[15] F. Hellmann, P. Schultz, P. Jaros, R. Levchenko, T. Kapitaniak, J. Kurths, and Y. Maistrenko, Network-induced multistability through lossy coupling and exotic solitary states, *Nature Communications* **11**, 592 (2020).

[16] S. Huang, Reprogramming cell fates: reconciling rarity with robustness, *BioEssays* **31**, 546 (2009).

[17] P. J. Menck, J. Heitzig, N. Marwan, and J. Kurths, How basin stability complements the linear-stability paradigm, *Nature Physics* **9**, 89 (2013).

[18] M. S. Soliman and J. M. T. Thompson, Global dynamics underlying sharp basin erosion in nonlinear driven oscillators, *Physical Review A* **45**, 3425 (1992).

[19] C. S. Holling, Resilience and Stability of Ecological Systems, *Annual Review of Ecology and Systematics* **4**, 1 (1973), publisher: Annual Reviews.

[20] H. Krakovská, C. Kuehn, and I. P. Longo, Resilience of dynamical systems, *European Journal of Applied Mathematics* **35**, 155 (2024).

[21] C. Kuehn, *Multiple Time Scale Dynamics*, Vol. 191 (Springer-Verlag GmbH, 2015).

[22] M. Krupa, B. Sandstede, and P. Szmolyan, Fast and Slow Waves in the FitzHugh–Nagumo Equation, *Journal of Differential Equations* **133**, 49 (1997).

[23] J. Balzer, R. Berner, K. Lüdge, S. Wieczorek, J. Kurths, and S. Yanchuk, Canard Cascading in Networks with Adaptive Mean-Field Coupling, *Physical Review Letters* **133**, 237401 (2024).

[24] P. D. L. Ritchie, H. Alkhayouon, P. M. Cox, and S. Wieczorek, *Chaos: An Interdisciplinary Journal of Nonlinear Science* **35** (2025).

zorek, Rate-induced tipping in natural and human systems, *Earth System Dynamics* **14**, 669 (2023).

[25] M. Desroches, J. Guckenheimer, B. Krauskopf, C. Kuehn, H. M. Osinga, and M. Wechselberger, Mixed-Mode Oscillations with Multiple Time Scales, *SIAM Review* **54**, 211 (2012).

[26] R. Berner, T. Gross, C. Kuehn, J. Kurths, and S. Yanchuk, Adaptive dynamical networks, *Physics Reports* **1031**, 1 (2023).

[27] R. Berner, S. Vock, E. Schöll, and S. Yanchuk, Desynchronization Transitions in Adaptive Networks, *Physical Review Letters* **126**, 028301 (2021).

[28] J. Fialkowski, S. Yanchuk, I. M. Sokolov, E. Schöll, G. A. Gottwald, and R. Berner, Heterogeneous Nucleation in Finite-Size Adaptive Dynamical Networks, *Physical Review Letters* **130**, 067402 (2023).

[29] O. V. Maslennikov and V. I. Nekorkin, Hierarchical transitions in multiplex adaptive networks of oscillatory units, *Chaos* **28**, 10.1063/1.5077075 (2018).

[30] T. Gross and B. Blasius, Adaptive coevolutionary networks: a review, *Journal of The Royal Society Interface* **5**, 259 (2008).

[31] T. Aoki and T. Aoyagi, Self-organized network of phase oscillators coupled by activity-dependent interactions, *Phys. Rev. E* **84**, 66109 (2011).

[32] V. Röhr, R. Berner, E. L. Lameu, O. V. Popovych, and S. Yanchuk, Frequency cluster formation and slow oscillations in neural populations with plasticity, *PLOS ONE* **14**, e0225094 (2019).

[33] C. K. R. T. Jones, Geometric singular perturbation theory, in *Dynamical Systems: Lectures Given at the 2nd Session of the Centro Internazionale Matematico Estivo (C.I.M.E.) held in Montecatini Terme, Italy, June 13–22, 1994*, edited by L. Arnold, C. K. R. T. Jones, K. Mischaikow, G. Raugel, and R. Johnson (Berlin, Heidelberg, 1995) pp. 44–118.

[34] M. Wechselberger, *Geometric Singular Perturbation Theory Beyond the Standard Form*, Frontiers in Applied Dynamical Systems: Reviews and Tutorials, Vol. 6 (Cham, 2020).

[35] N. Fenichel, Geometric singular perturbation theory for ordinary differential equations, *Journal of Differential Equations* **31**, 53 (1979).

[36] M. Krupa and P. Szmolyan, Relaxation Oscillation and Canard Explosion, *Journal of Differential Equations* **174**, 312 (2001).

[37] F. Hummel, P. Ashwin, and C. Kuehn, Reduction methods in climate dynamics—A brief review, *Physica D: Nonlinear Phenomena* **448**, 133678 (2023).

[38] K. Hasselmann, Stochastic climate models Part I. Theory, *Tellus* **28**, 473 (1976).

[39] A. Politi, S. Yanchuk, and G. Giacomelli, Nearly Hamiltonian dynamics of laser systems, *Physical Review Research* **5**, 023059 (2023).

[40] Y. Kuznetsov, *Elements of Applied Bifurcation Theory*, Vol. 112 (1995) series Title: Applied Mathematical Sciences.

[41] See Supplemental Material at URL-will-be-inserted-by-publisher for the additional details.

[42] I. Franović, S. Yanchuk, S. Eydam, I. Baćić, and M. Wolfrum, Dynamics of a stochastic excitable system with slowly adapting feedback, *Chaos: An Interdisciplinary Journal of Nonlinear Science* **30**, 083109 (2020).

[43] This corresponds to the case of unboundedly growing $\varphi(t)$ when φ considered on a real line \mathbb{R} or, equivalently, rotating on a circle \mathbb{S}^1 when φ considered modulo 2π phase.

[44] S. H. Strogatz, *Nonlinear Dynamics and Chaos: with Applications to Physics, Biology, Chemistry, and Engineering* (Addison-Wesley, 1994).

[45] S. H. Park and S. Kim, Noise-induced phase transitions in globally coupled active rotators, *Physical Review E* **53**, 3425 (1996).

[46] B. Lindner, Effects of noise in excitable systems, *Physics Reports* **392**, 321 (2004).

[47] A. V. Dolmatova, D. S. Goldobin, and A. Pikovsky, Synchronization of coupled active rotators by common noise, *Physical Review E* **96**, 062204 (2017).

[48] V. V. Klinshov, D. A. Zlobin, B. S. Maryshev, and D. S. Goldobin, Effect of noise on the collective dynamics of a heterogeneous population of active rotators, *Chaos: An Interdisciplinary Journal of Nonlinear Science* **31**, 043101 (2021).

[49] R. Ronge and M. A. Zaks, Emergence and stability of periodic two-cluster states for ensembles of excitable units, *Physical Review E* **103**, 012206 (2021).

[50] O. Burylko, M. Wolfrum, S. Yanchuk, and J. Kurths, Time-reversible dynamics in a system of two coupled active rotators, *Proceedings of the Royal Society A: Mathematical, Physical and Engineering Sciences* **479**, 20230401 (2023).

[51] B. Schäfer, D. Witthaut, M. Timme, and V. Latora, Dynamically induced cascading failures in power grids, *Nature Communications* **9**, 1 (2018).

[52] O. D’Huys, R. Veltz, A. Dolcemascolo, F. Marino, and S. Barland, Canard resonance: on noise-induced ordering of trajectories in heterogeneous networks of slow-fast systems, *Journal of Physics: Photonics* **3**, 024010 (2021).

[53] M. Ciszak, F. Marino, A. Torcini, and S. Olmi, Emergent excitability in populations of nonexcitable units, *Physical Review E* **102**, 1 (2020).

[54] T. Song, H. Kim, S.-W. Son, and J. Jo, Synchronization of active rotators interacting with environment, *Physical Review E* **101**, 022613 (2020).

[55] M. Ciszak, S. Olmi, G. Innocenti, A. Torcini, and F. Marino, Collective canard explosions of globally-coupled rotators with adaptive coupling, *Chaos, Solitons & Fractals* **153**, 111592 (2021).

[56] L. G. Venegas-Pineda, H. Jardón-Kojakhmetov, and M. Cao, Stable chimera states: A geometric singular perturbation approach, *Chaos: An Interdisciplinary Journal of Nonlinear Science* **33** (2023).

[57] M. Krupa and P. Szmolyan, Extending geometric singular perturbation theory to nonhyperbolic points—fold and canard points in two dimensions, *SIAM Journal on Mathematical Analysis* **33**, 286 (2001).

Supplemental Material

I. DETAILS OF THE NUMERICAL METHODS

A. The singular funnel volume using Monte Carlo simulations in Figures 2 and 3

We estimated the volume of the singular funnel in Figures 2 and 3 of the main paper by Monte Carlo simulations as follows:

- For each value of ε , we randomly choose a large number M of uniformly distributed initial conditions, with $\varphi_i(0) \in [0, 2\pi]$ and $\mu(0) \in [-10, 0]$.
- For each of these initial conditions, we numerically solve the initial value problem consisting of system (5)–(6) or (9)–(10) and the initial condition, for a long enough time. For the numerical integration we use the MATLAB function `ode45`, with `RelTol` = 10^{-10} and `AbsTol` = 10^{-10} . The time span for our integration is $[0, 10/\varepsilon]$.
- We then determine whether the solution trajectory converges to the stable equilibrium e_1 or to the rotating periodic orbit γ_c . To detect convergence, we use a user-defined event function to stop the integration at time t_{end} when $\mu(t_{\text{end}}) > 9$. If this condition applies, then the solution has converged to γ_c otherwise, it has converged to e_1 .
- The volume V of the basin of attraction of the limit cycle γ_c is then given by

$$V = \frac{K}{M},$$

where K is the number of initial conditions whose solution trajectories converge to γ_c over time.

B. Numerical averaging in Figure 3

We computed the potential of the average system of the two oscillator network in Figure 3 as follows:

- For fixed parameter values of $\omega_{1,2}$, κ , η , α , and a given value of μ , we randomly choose initial values for $\varphi_1(0)$ and $\varphi_2(0)$ from the interval $[0, 2\pi]$.
- We consider the (fast) layer problem of system (5)–(6)], which is given as:

$$\dot{\varphi}_i = \omega_i + \mu - \sin \varphi_i + \frac{\kappa}{N} \sum_{j=1}^N \sin(\varphi_j - \varphi_i), \quad i = 1, 2. \quad (11)$$

- The initial value problem consisting of system (11) and the randomly chosen initial condition $(\varphi_1(0), \varphi_2(0))$ was solved numerically for a sufficiently long time interval $[0, 600]$. For the numerical integration, the MATLAB function `ode45` was used, with `RelTol` = 10^{-10} and `AbsTol` = 10^{-10} .
- The transient part $t \in [0, 100]$ of the solution was discarded to ensure that the solution has converged to an invariant state.
- We compute $X(t) = \frac{1}{2} \sum_{j=1}^2 \sin(\varphi_j(t) + \alpha)$ for $t \in [100, 600]$ and write the average system as:

$$\dot{\mu} = \bar{g}(\mu) = \frac{1}{500} \int_{100}^{600} (-\mu + \eta(1 - X(t))) \, dt \quad (12)$$

The definite integral on the right-hand side was computed numerically using the trapezoidal rule.

- The potential $U(\mu)$ is given by:

$$U(\mu) = \int_0^\mu \bar{g}(s) \, ds.$$

II. SUPERCRITICAL PITCHFORK NORMAL FORM WITH ADAPTIVE PARAMETER

The pitchfork normal form with adaptively changing parameter, as introduced in the manuscript, is given by

$$\dot{x}(t) = x(\mu - x^2), \quad x \geq 0, \quad (13)$$

$$\dot{\mu}(t) = \varepsilon(-\mu + ax - b), \quad (14)$$

where $\varepsilon > 0$ is a small parameter, and $a, b > 0$ are parameters determining the linear adaptation function.

First we consider the equilibria of the fast system (13), which, when considered as a set in the phase space (x, μ) of the fast-slow system (13)–(14), define the critical manifolds

$$S_0 = \{(x, \mu) \in [0, \infty) \times \mathbb{R} : x = 0\}, \quad (15)$$

$$S_1 = \{(x, \mu) \in [0, \infty) \times \mathbb{R} : x = \sqrt{\mu}, \mu \geq 0\}. \quad (16)$$

Linearization of the vector field along these manifolds shows that S_0 has two branches, namely

$$S_0^a = \{(x, \mu) \in [0, \infty) \times \mathbb{R} : x = 0, \mu < 0\}, \quad (17)$$

$$S_0^r = \{(x, \mu) \in [0, \infty) \times \mathbb{R} : x = 0, \mu > 0\}, \quad (18)$$

which are locally attracting and repelling respectively and such that $S_0 = S_0^a \cup \{0\} \cup S_0^r$, while S_1 is locally attracting. This stability information is shown in Fig. 5(b) by solid lines for the stable parts and dashed line for the unstable part of the critical manifolds respectively.

Thus the fast system (13) has a unique stable equilibrium for all values of the slow variable μ , which is attracting all values of $x \geq 0$ for $\mu \leq 0$ and all $x > 0$ for $\mu > 0$. Therefore we consider the reduced slow system on the union of the corresponding stable parts of the critical manifolds. We substitute

$$x = \sqrt{\mu}H(\mu) = \begin{cases} 0, & \mu \leq 0 \\ \sqrt{\mu}, & \mu > 0, \end{cases} \quad (19)$$

into (14) and obtain

$$\dot{\mu} = \varepsilon \begin{cases} -\mu - b, & \mu \leq 0 \\ -\mu + a\sqrt{\mu} - b, & \mu > 0, \end{cases} \quad (20)$$

or in a more compact form

$$\dot{\mu} = \varepsilon(-\mu + aH(\mu)\sqrt{\mu} - b), \quad (21)$$

where $H(\mu)$ is the Heaviside step function.

We consider the case when the reduced system (21) has three equilibria e_0 , e_1 , and e_2 as shown in Fig. 5, their μ coordinates are $\mu_0 < 0$, $\mu_1 > 0$, and $\mu_2 > 0$, respectively. Requiring three equilibria leads to the following conditions on the parameters:

$$b > 0 \quad \text{and} \quad a > 2\sqrt{b}. \quad (22)$$

Under the conditions (22), the reduced system (21) is bistable with two stable equilibria e_0 , e_2 and one unstable equilibrium e_1 :

$$e_0 : (0, -b), \quad e_{1,2} : \left(\sqrt{\mu}, \frac{a}{2} \pm \sqrt{\left(\frac{a}{2}\right)^2 - b} \right). \quad (23)$$

The potential of system (21) can be calculated as the integral of its right-hand side, leading to

$$U(\mu) = \frac{\mu^2}{2} + b\mu - \frac{2}{3}a\mu\sqrt{\mu}H(\mu), \quad (24)$$

where, for simplicity, we dropped the scaling factor ε .

The equilibria e_0 and e_2 are stable in the phase space of the full system (13)–(14). The attraction basins for these equilibria are separated by the stable manifolds $W_{1,2}^s(e_1)$ of the saddle equilibrium e_1 , see Fig. 5 and Fig. 1(a) of the main manuscript. For our purposes, it is worth noting that the manifold $W_2^s(e_2)$ converges exponentially to $x = 0$ as $\mu \rightarrow \infty$. As a result, a part of the attraction basin of the equilibrium e_0 extends into an exponentially small region for all $\mu > 0$, which we call **singular funnel**.

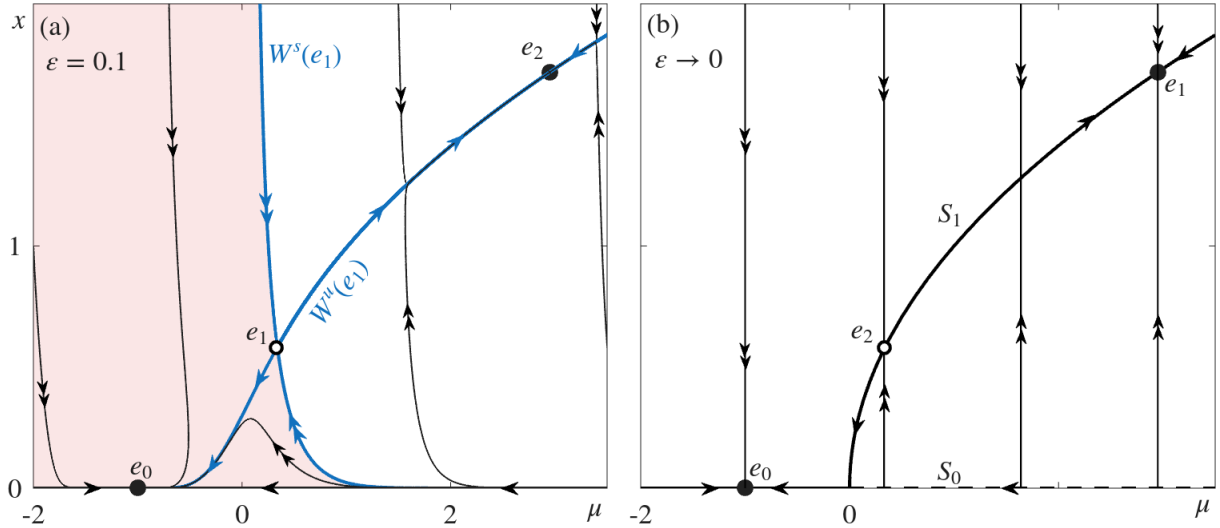


FIG. 5. Phase portrait of the pitchfork normal form, system (13)–(14). (a) $\varepsilon = 0.1$, the red region (white) region is the basin of attraction of $e_0(e_2)$, the stable $W^s(e_1)$ (unstable $W^u(e_1)$) manifolds of the saddle point e_1 in blue. (b) $\varepsilon \rightarrow 0$, critical manifolds $S_{0,1}$ in thick black, the attracting parts in solid and the repelling part of S_0 is dashed. The double arrowed vertical black lines indicate the direction of the fast layer system. Parameters: $a = 3$, $b = 2$.

III. A MODEL WITHOUT CRITICAL MANIFOLD CROSSING

Another system of equations introduced in the manuscript is

$$\dot{x}(t) = x (\tanh \mu + 2 - x), \quad (25)$$

$$\dot{\mu}(t) = \varepsilon(-\mu + ax - b). \quad (26)$$

The corresponding reduced system on the stable critical manifold (adiabatic elimination) is given by

$$\dot{\mu}(t) = \varepsilon(-\mu - b + a(\tanh(\mu) + 2)), \quad (27)$$

and the corresponding (rescaled) potential V is

$$\begin{aligned} U &= - \int (a \tanh(\mu) - \mu - b + 2a) d\mu \\ &= \mu^2/2 - (2a - b)\mu - a \ln(\cosh(\mu)). \end{aligned}$$

IV. ADAPTIVE PHASE ROTATOR

A. Timescale reduction

The adaptive phase rotator considered in the manuscript has the form

$$\dot{\varphi} = \omega + \mu - \sin \varphi, \quad (28)$$

$$\dot{\mu} = \epsilon(-\mu + \eta(1 - \sin(\varphi + \alpha))). \quad (29)$$

The slow-fast dynamics of this system for $\alpha = 0$ was studied in [42], for the deterministic and stochastic case. Here we extend these results (for the deterministic case) to $\alpha \neq 0$.

The critical manifold has the form:

$$S_0 := \{(\mu, \varphi) : \mu = -\omega + \sin \varphi\}, \quad (30)$$

and it exists in the stripe $|\mu + \omega| \leq 1$. To obtain the dynamics on this critical manifold (adiabatic elimination), we substitute $\sin \varphi = \mu + \omega$ into (29), leading to

$$\dot{\mu} = -\mu + \eta \left(1 - (\mu + \omega) \cos \alpha \mp \sqrt{1 - (\mu + \omega)^2} \sin \alpha \right), \quad |\mu + \omega| \leq 1. \quad (31)$$

For $|\mu + \omega| > 1$, the fast subsystem (28) has no equilibria, but exhibits periodic rotation described by

$$\varphi_\mu(t) = 2 \arctan \left(\frac{1 + \Omega(\mu) \tan \left(\frac{t}{2} \Omega(\mu) \right)}{\omega + \mu} \right),$$

where

$$\Omega(\mu) = \sqrt{(\omega + \mu)^2 - 1}.$$

To average the slow dynamics (29) along these fast rotations, we need to average the oscillating term $\sin(\varphi(t) + \alpha)$ over the period $T = 2\pi/\Omega$:

$$\begin{aligned} \langle \sin(\varphi_\mu(t) + \alpha) \rangle &= \frac{1}{T} \int_0^{2\pi/\Omega} \sin(\varphi_\mu(t) + \alpha) dt = \\ &= \frac{1}{T} \cos \alpha \int_0^T \sin \varphi_\mu(t) dt + \frac{1}{T} \sin \alpha \int_0^T \cos \varphi_\mu(t) dt = \\ &= ((\omega + \mu) - \Omega) \cos \alpha + \frac{1}{T} \sin \alpha \int_0^T \cos \varphi_\mu(t) dt \\ &= ((\omega + \mu) - \Omega) \cos \alpha + \frac{1}{T} \sin \alpha \int_0^{2\pi} \frac{\cos \varphi d\varphi}{\omega + \mu - \sin \varphi} = \\ &= ((\omega + \mu) - \Omega) \cos \alpha + \frac{1}{T} \sin \alpha \int_0^{2\pi} \frac{d \sin \varphi}{\omega + \mu - \sin \varphi} = \\ &= ((\omega + \mu) - \Omega) \cos \alpha. \end{aligned}$$

Therefore, the averaged equation is

$$\dot{\mu} = -\mu + \eta \left(1 - \left((\omega + \mu) - \sqrt{(\omega + \mu)^2 - 1} \right) \cos \alpha \right), \quad |\omega + \mu| > 1. \quad (32)$$

Finally, we combine the reduced systems (31) for $|\mu + \omega| \leq 1$ and (32) for $|\mu + \omega| > 1$, to obtain

$$\dot{\mu} = -\mu + \eta (1 - (\mu + \omega) \cos \alpha + \Omega(\mu)), \quad (33)$$

where

$$\Omega(\mu) = \begin{cases} \sqrt{1 - (\mu + \omega)^2} \sin \alpha, & |\mu + \omega| \leq 1 \\ \sqrt{(\omega + \mu)^2 - 1} \cos \alpha, & |\mu + \omega| > 1. \end{cases} \quad (34)$$

The equilibria of the averaged dynamics satisfy

$$-\mu + \eta (1 - (\mu + \omega) \cos \alpha + \Omega(\mu)) = 0. \quad (35)$$

B. Parameter region for singular basin

In Figure 6, we present the bifurcations of system (28)–(29) with respect to the parameters α and ε . In the parameter region we examined, there are two Hopf bifurcation curves and three homoclinic curves. Also, the system has two equilibrium solutions e_1 and e_2 , and up to four periodic solutions: $\gamma_{1,2}$, which are regular limit cycles, and $\gamma_{c,u}$, which are rotating limit cycles resulting from the fact that $\varphi \in [0, 2\pi]$. We point out that the rotating limit cycle γ_c is always stable in the parameter region under examination.

If we consider Figure 6 (a), starting from the left-hand side, we have a monostable system in region (b), Figure 6 (b), where the equilibrium e_1 is unstable. At the subcritical Hopf curve H_1 , the unstable equilibrium e_1 gains stability in region (c), Figure 6 (c), and an unstable limit cycle γ_1 emerges to form the boundary of the basin of attraction of e_1 .

The unstable limit cycle γ_1 intersects the saddle equilibrium e_2 at the homoclinic bifurcation h_1 , Figure 6 (d). To the right-hand side of h_1 , region (g), the basin of attraction of the rotating limit cycle is singular, with the boundary given by the stable manifold of the saddle e_2 , Figure 6 (g).

The second homoclinic bifurcation, h_2 , is formed by the intersection of the unstable rotating limit cycle γ_u and the saddle equilibrium e_2 , Figure 6 (g). Region (e), Figure 6 (e), below the curve h_2 , is a bistable region where both the equilibrium e_1 and the rotating limit cycle γ_c are stable, and the basin boundary is given by the unstable rotating limit cycle γ_u . The second Hopf bifurcation, H_2 , is supercritical. The stable equilibrium e_1 in Figure 6 (g) loses stability, giving rise to a stable limit cycle γ_2 , Figure 6 (h). The basin of attraction of γ_c is still singular in region (h). The region of singular basin ends at the homoclinic bifurcation h_3 , Figure 6 (i), where the stable limit cycle γ_2 intersects the saddle equilibrium e_2 . In region (j), Figure 6 (j), the system is monostable again, where the rotating limit cycle γ_c is the only stable attractor.

C. Analytical considerations for the singular funnel scaling

Here we provide some analytical considerations, which substantiate the scaling given in the main manuscript as equation (8).

Consider $\varepsilon \ll 1$ and the boundaries of the singular basin to be

$$\phi_u(t) = \phi(t, \phi_{u0}, \mu_0), \quad \mu_u(t) = \phi(t, \phi_{u0}, \mu_0)$$

for the upper, and

$$\phi_l(t) = \phi(t, \phi_{l0}, \mu_0), \quad \mu_l(t) = \phi(t, \phi_{l0}, \mu_0)$$

for the lower boundaries. Here $\phi_{l0} < \phi_{u0}$, $-\omega - 1 < \mu_0 < \mu(e_2)$ are some chosen points on the singular funnel such that $\phi(0, \phi_{X0}, \mu_0) = \phi_{X0}$ and $\mu(0, \phi_{X0}, \mu_0) = \mu_0$ for $X \in \{u, l\}$. For any fixed $\delta < \phi_{u0} - \phi_{l0}$, there exists $t_0 < 0$ such that

$$\phi_l(t_0) - \phi_u(t_0) = \delta$$

due to the contraction to the equilibrium of the layer system (fast equation (28)) in the backwards time.

Being δ -close to the equilibrium of the fast system, it can be linearized for $t_f < t < t_0$, where t_f is the time when the system approaches the fold point of the layer equation. This leads to

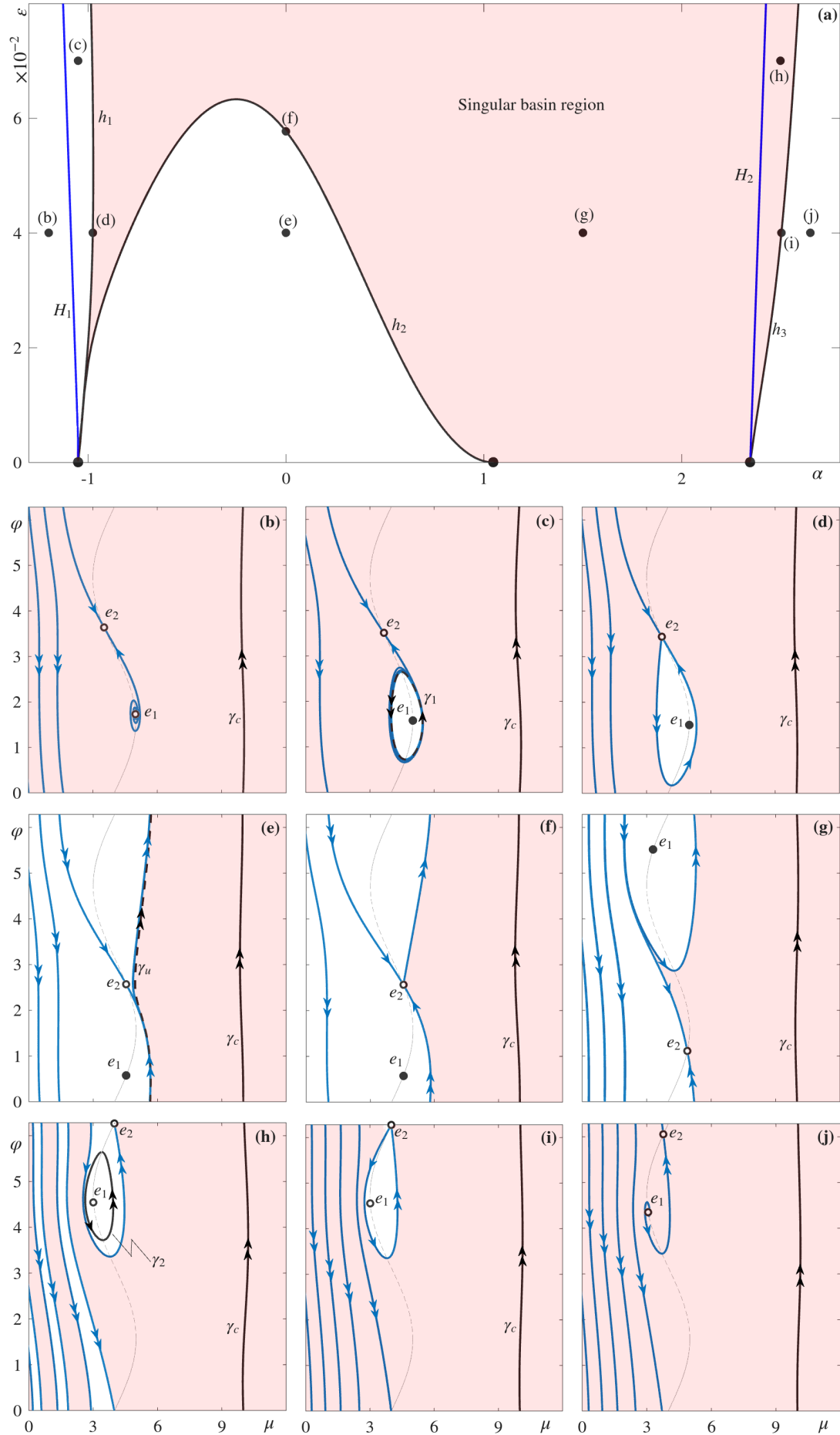
$$\begin{aligned} \dot{\phi} &= \omega + \mu - \sin(\phi^*(\mu)) - \cos(\phi^*(\mu))(\phi - \phi^*(\mu)), \\ \dot{\mu} &= \epsilon(-\mu + \eta(1 - \sin(\phi^*(\mu) + \alpha)) - \cos(\phi^*(\mu) + \alpha))(\phi - \phi^*(\mu)). \end{aligned}$$

Taking into account that $\phi^*(\mu)$ is the critical manifold, the leading terms in both equations read as:

$$\begin{aligned} \dot{\phi} &= -\cos(\phi^*(\mu))(\phi - \phi^*(\mu)), \\ \dot{\mu} &= \epsilon(-\mu + \eta(1 - \sin(\phi^*(\mu) + \alpha))). \end{aligned}$$

Denoting $\Delta = \phi_u - \phi_l$, we have

$$\begin{aligned} \dot{\Delta}(t) &= -\cos(\phi^*(\mu))\Delta(t), \\ \dot{\mu}(t) &= \epsilon(-\mu + \eta(1 - \sin(\phi^*(\mu) + \alpha))). \end{aligned}$$

FIG. 6. Two-parameter (α, ε) bifurcation diagram for system (28)–(29), with examples of phase portraits.

The above equations give $d\Delta/dt$ and $d\mu/dt$. Hence we obtain $d\Delta/d\mu$ as follows

$$\frac{d\Delta}{d\mu} = \frac{1}{\epsilon} \frac{-\cos(\phi^*(\mu))}{-\mu + \eta(1 - \sin(\phi^*(\mu) + \alpha))} \Delta,$$

which can be solved as

$$\Delta(\mu) = \Delta(\mu_0) \exp \left[\frac{1}{\epsilon} \int_{\mu_0}^{\mu} \frac{\cos(\phi^*(\mu))}{\mu - \eta(1 - \sin(\phi^*(\mu) + \alpha))} d\mu \right] = \Delta(\mu_0) \exp \left[-\varepsilon^{-1} C(\mu, \mu_0) \right], \quad (36)$$

which provides the scaling as in equation (8) of the main paper.

In addition, according to [57], there is only an algebraic contraction of the singular funnel stripe across the fold point. Hence, the exponential estimate (36) remains for the further motion along the fast flow.